Journal of Hazardous Materials 494 (2025) 138449

Contents lists available at ScienceDirect

Journal of Hazardous Materials

journal homepage: www.elsevier.com/locate/jhazmat

Skin biocompatibility of hexagonal boron nitride: An *in vitro* study on HaCaT keratinocytes and 3D reconstructed human epidermis

Michela Carlin [a], Silvio Sosa [a], Viviana Jehová González [b,c], Aurelia Tubaro [a], Ester Vázquez [b,c], Maurizio Prato [d,e,f], Marco Pelin [a,*]

[a] Department of Life Sciences, University of Trieste, Trieste 34127, Italy
[b] Regional Institute of Applied Scientific Research (IRICA), University of Castilla-La Mancha, Ciudad Real 13005, Spain
[c] Department of Organic Chemistry, Faculty of Science and Chemistry Technologies, University of Castilla-La Mancha, Ciudad Real 13005, Spain
[d] Department of Chemical and Pharmaceutical Sciences, University of Trieste, Trieste 34127, Italy
[e] Center for Cooperative Research in Biomaterials (CIC biomaGUNE), Basque Research and Technology Alliance (BRTA), Donostia-San Sebastian 20014, Spain
[f] Basque Foundation for Science (IKERBASQUE), Bilbao 48009, Spain

HIGHLIGHTS

- hBN induces low cytotoxicity despite its high internalization into keratinocytes.
- hBN affects the same cellular parameters altered by graphene, with a lower potency.
- hBN is not skin corrosive.
- hBN is not skin irritant.
- hBN pro-inflammatory potential is extremely low at the skin level.

GRAPHICAL ABSTRACT

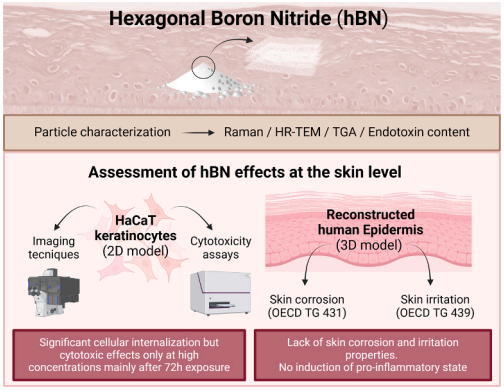

ARTICLE INFO

Keywords:
2D materials
Dermotoxicity
OECD guidelines
Inflammation
Hazard characterization

ABSTRACT

Hexagonal boron nitride (hBN) is a promising two-dimensional (2D) material of interest to the scientific community and industry due to its revolutionary physico-chemical features. Skin contact is one of the most feasible exposure routes both for workers, producing hBN, and consumers, using hBN-enabled nanotechnologies. Hence, the toxic potential of hBN at the cutaneous level was evaluated following an *in vitro* approach with different degree of complexity, using a simplified cell model (HaCaT keratinocytes), and a more predictive and complete skin tissue (a 3D model of human epidermis). Despite its significant uptake by keratinocytes, hBN exerted only weak adverse effects, such as slight alterations of cells parameters indices of cytotoxicity (cell viability, cell mass and plasma membrane integrity) and mitochondrial-related dysfunctions (mitochondrial depolarization, ATP depletion and reactive oxygen species production), detectable only at high concentrations (>25 μg/mL) and mainly after a long exposure (72 h). In addition, adoption of the OECD TG 431 and 439 on the 3D reconstructed

* Corresponding author.
E-mail address: mpelin@units.it (M. Pelin).

https://doi.org/10.1016/j.jhazmat.2025.138449
Received 3 February 2025; Received in revised form 7 April 2025; Accepted 29 April 2025
Available online 30 April 2025

human epidermis model demonstrated hBN as a non-corrosive and non-irritant material, with an extremely low pro-inflammatory potential. These results denote a good biocompatibility of hBN at the skin level.

1. Introduction

Two-dimensional (2D) nanomaterials are a diverse class of materials possessing advantageous physico-chemical properties, such as atomic-thin morphology, broad surface area and layered structure [43]. Looking beyond the well-studied graphene, a wide number of 2D nanomaterials has been explored [49]. One of them is hexagonal boron nitride (hBN), known as "white graphene", consisting in a hexagonal sp^2-bonded network with strong in-plane polar bonds between nitrogen and boron atoms [31]. Due to its chemical structure, hBN exhibits chemical inertness, unique mechanical properties, superb thermal conductivity, oxidation stability and piezoelectric properties. Moreover, atomic films of hBN show insulating properties with consistent energy band-gap and transparency over a wide wavelength range [3,31,67,73,8]. All these features open up new scenarios for innovative applications and attract considerable interest as insulator [12,35], lubricant additive [17], heat dissipator for electronic devices [33,45] and textile component [79], but also in biomedical fields, such as drug delivery and cancer therapy [15,52,71], and cosmetics [26].

Although hBN may allow solutions to current challenges in many technological fields, scientific concern for human health safety cannot be excluded considering the occupational and/or consumer exposure to this material. In particular, one of the most important exposure routes for 2D nanomaterials could be the cutaneous one [23,42,60]. To date, even though some *in vitro* studies on the cutaneous effects of other boron nitride (BN) allotropes (such as BN nanotubes and BN quantum dots) on skin fibroblasts [14,19–21,65,69] and keratinocytes [25,77] are available, only few studies report the cutaneous effects of the corresponding 2D nanoform (hBN). The effects of hBN (0.025–0.4 mg/mL) were firstly assessed on human normal skin fibroblasts by means of metabolic activity, DNA and protein cellular content, recording only mild effects after 24 and 48 h exposure to high concentrations (0.2–0.4 mg/mL) [38]. Another study on human dermal fibroblasts demonstrated that hBN did not impact cell viability up to 100 μg/mL, with significant effects only at high concentrations (150.0–500.0 μg/mL). Moreover, non-toxic hBN concentrations increased fibroblasts proliferation and migration, improving wound healing process, also by lowering reactive oxygen species (ROS) production [70]. In addition, different studies evaluated the effects of hBN and different hBN-containing composites/hybrid materials on HaCaT keratinocytes [1,50,7]. In the effort to assess its antibacterial activity, cytotoxicity of a composite made of polyhydroxyalkanoate, chitosan and hBN (1.0 %) was evaluated on HaCaT cells. Using the lactate dehydrogenase (LDH) release assay, this material showed no cytotoxic effects on keratinocytes [50]. Later, studying amoebicidal effects of a nanocomposite made of polyaniline and hBN (PANI/hBN), Abdelnasir and colleagues found that hBN alone exhibited a minimal cytotoxicity at concentrations up to 83.3 μg/mL, in terms of LDH release [1]. Lastly, a recent work demonstrated the optimal cutaneous biocompatibility of hBN and a relevant thermoplastic polyurethane composite (TPU-hBN) across their life cycle. Despite evidence of cellular uptake, no major effects at the cellular level (in terms of cell viability, pro-inflammatory response and changes of proteomic/metabolomic profiles) were found in keratinocytes exposed up to 4 weeks to pristine or photo-chemically degraded hBN or TPU-hBN composite [7].

Considering the relevance of hBN cutaneous exposure and the limited data on its effects at the skin level currently available, this study is aimed at deeply investigating the potential cutaneous toxicity of hBN, using HaCaT keratinocytes as *in vitro* immortalized human non-tumor cell model, broadly adopted as a screening tool to assess skin toxicity of several substances [30]. Furthermore, to provide robust and reliable toxicological data, an *in vitro* three-dimensional (3D) model of Reconstructed human Epidermis (RhE) was used following specific test guidelines (TGs) established by the Organization for Economic Co-operation and Development (OECD), to assess skin corrosion and irritation, as two of the most important adverse outcomes at the cutaneous level.

2. Materials and methods

2.1. Materials

The hBN 2D material was synthesized using bulk boron nitride, which was exclusively sourced from Sigma-Aldrich (Milan, Italy). Glycine, also obtained from Sigma-Aldrich (Milan, Italy), was used as exfoliating agent of the bulk material.

If not otherwise specified, all reagents for *in vitro* experiments were purchased from Sigma-Aldrich (Milan, Italy).

2.2. Preparation and characterization of hBN

hBN 2D material was obtained through a mechanochemical approach, using bulk boron nitride as the precursor and glycine as the exfoliating agent [32]. In a typical procedure, bulk boron nitride (75 mg) and glycine (2.5 g) were placed in a 250 mL stainless steel jar containing 15 stainless steel balls (diameter: 2 cm). The mixture underwent mechanochemical processing in a Retsch PM100 ball-milling machine at 250 rpm for 15 min. The resulting material was dispersed in 100 mL water and subjected to dialysis at 70°C, with five solution changes every 90 min and one additional change left overnight. Then, the dispersion was freeze dried at −80°C and 0.005 bar, yielding the hBN 2D material in powdered form.

For experiments on HaCaT cells, hBN powder was suspended in sterile and endotoxin-free MilliQ water to obtain a 2 mg/mL stock suspension. Before use, the suspension was vortexed and sonicated by a bath sonicator for 10 min. Stock dispersions were further diluted in cell culture medium for cell exposure. For experiments on the 3D RhE model, hBN was tested directly as powder, put above the epidermis surface grown at the air-liquid interface.

2.3. Characterization of hBN

2.3.1. Raman spectroscopy

Raman spectra were obtained using an InVia Renishaw microspectrometer equipped with a 785 nm laser source (1 mW/μm^2). To ensure reproducibility, measurements were taken at 30–40 randomly selected points across the surface of the nanomaterial.

2.4. Thermogravimetric analysis (TGA)

Thermal stability was assessed using a TGA Q50 instrument (TA Instruments) under nitrogen, increasing the temperature from 100 °C to 800 °C, at a uniform rate of 10 °C per minute.

2.5. High-resolution transmission electron microscopy (HR-TEM) analysis

Structural imaging was conducted with a JEOL 2100 HRTEM operating at 100 kV. Samples were prepared by depositing a stable, diluted dispersion of hBN onto Lacey copper grids (3.00 mm, 200 mesh) via a dip-casting method, followed by drying under vacuum.

2.6. Detection of endotoxin content

2.6.1. Limulus amoebocyte lysate (LAL) assay

The presence of endotoxin (or lipopolysaccharide, LPS) in hBN was initially detected using a chromogenic LAL assay (Pierce™ Chromogenic Endotoxin Quantitation Kit; Thermo Fisher Scientific, Milan, Italy), which detection range was 0.1–1.0 endotoxin units/mL (EU/mL). To check the possible interference of hBN with the test, hBN samples were spiked with endotoxin at a concentration within the detection range (0.5 EU/mL) and submitted to the LAL assay. Measurements were performed following manufacturer's instructions. Results are reported as the mean LPS concentration (EU/mL) ± standard error (SE) in each sample.

2.6.2. Tumor necrosis factor (TNF)-α expression test (TET)

Endotoxin presence in hBN was evaluated also by a modified TET assay, as previously described [51,61]. Briefly, THP-1 cells, differentiated to macrophages by 24 h exposure to phorbol-12-myristate-13-acetate (PMA; 50 nM), were exposed to a non-cytotoxic hBN concentration (12.5 μg/mL) for 24 h, with or without polymyxin B sulfate (10 μM). A standard curve, built on TNF-α cell release data, was then obtained exposing macrophages to LPS (0.01–100 ng/mL); 100 ng/mL LPS was included as internal control. Supernatants were then collected and TNF-α was quantified by ELISA, according to the manufacturer's instructions (Diaclone; Besançon, France). Quantitation of LPS in hBN was extrapolated by the standard curve. Results are reported as the mean LPS concentration (EU/mL) ± standard error (SE).

2.7. HaCaT cells

Immortalized human HaCaT keratocytes were obtained from Cell Line Service (DKFZ; Eppelheim, Germany). Cells were cultured in high-glucose Dulbecco's Modified Eagle's medium (DMEM) containing 10 % FBS, 2 mM L-glutamine, 100 IU/mL penicillin and 100 mg/mL streptomycin, at 37°C in a 5 % CO_2 atmosphere. Cell passage was performed when the culture reached confluence, once a week.

2.8. Structured illumination microscopy (SIM) analysis

HaCaT cells were seeded in complete growth medium and cultured for 24 h before exposure to hBN (50 μg/mL) for 24 and 72 h. This concentration corresponds to the lowest one that significantly altered the majority of the considered cell parameters, indices of cytotoxicity. Part of the samples were prepared as follows: plasma-membranes were stained with the 1,1′-Dioctadecyl-3,3,3′,3′-tetramethylindocarbocyanine perchlorate fluorescence probe (DiL; 1 μM) for 10 min at room temperature (RT). Then, cells were washed twice with phosphate buffer solution (PBS), fixed for 30 min in 4 % paraformaldehyde (PFA). After three washing steps with PBS, nuclei were stained with 2 μg/mL Hoechst reagent (Life Technologies; Milan, Italy) for 10 min. The other samples were fixed with PFA, as reported above, and cells were incubated with 0.1 M glycine for 5 min. After three washing steps with PBS, cells were permeabilized with 0.1 % Triton-X 100 for 5 min. Then, cells were washed three times and co-labelled with phalloidin-iFluor™ 488 conjugate (1:1000, Cayman Chemical; Ann Arbor, MI, USA) and 2 μg/mL Hoechst reagent (Life Technologies; Milan, Italy) for 10 min at RT to stain F-actin filaments and nuclei, respectively. Finally, all samples were mounted on 1 mm thick coverslips using Mowiol. Images were taken by a super-resolution structured illumination microscope (Elyra 7, Zeiss; Milan, Italy) at a 63x magnification, using the following channel setting: red fluorescence with excitation laser line 561 nm, green fluorescence with excitation laser line 488 nm and blue fluorescence with excitation laser line 405 nm. Nanomaterial images were acquired in bright field. The image-processing package Fiji was used for offline reconstructions of images and colors inversion.

2.9. Transmission electron microscopy (TEM) analysis

HaCaT cells were seeded in complete growth medium one day before exposure to hBN (50 μg/mL) for 24 and 72 h. Thereafter, control and exposed cells were detached by trypsinization, centrifuged, and resuspended in 2.5 % glutaraldehyde (Electron Microscopy Sciences; Hatfield, PA, USA) in 0.1 M phosphate buffer. After 1 h incubation, each sample was immersed in a 1 % solution of osmium tetroxide in 0.1 sodium phosphate buffer for 1 h, at 4°C. Subsequently, samples were dehydrated using a gradient of ethanol, followed by propylene oxide, and embedded in epoxy resin (Durcupan™ ACM). Ultrathin sections (70–90 nm) were prepared using a UltraCut Microtome (Reichert-Jung; Depew, NY, USA) and were further contrasted with UranyLess (Electron Microscopy Sciences; Hatfield, PA, USA) and lead citrate (Electron Microscopy Sciences; Hatfield, PA, USA). Samples were examined using a Philips FEI EM208 transmission electron microscope. Acquisition of images was carried out using the digital camera QUEMESA and the RADIUS 2.0 EMSIS software.

2.10. WST-8 assay

Viability of HaCaT cells was assessed by the 2-(2-methoxy-4-nitrophenyl)-3-(4-nitrophenyl)-5-(2,4-disulfophenyl)-2 H-tetrazolium (WST-8) reduction assay (Cell Counting Kit-8 assay; Sigma-Aldrich; Milan, Italy). HaCaT cells exposed to hBN (0.8–400.0 μg/mL) for 24 and 72 h were washed thrice with PBS (200 μL/well) before incubation with fresh medium containing 10 % WST-8 reagent for 4 h. Absorbance was measured at 450 nm by the FLUOstar® Omega microplate reader (BMG LABTECH; Ortenberg, Germany). Data are reported as % of cell viability, as compared to negative control (HaCaT cells not exposed to hBN).

2.11. Sulforhodamine B assay

Cell mass, as index of viable adhered cells, was assessed by the Sulforhodamine B (SRB) assay. Briefly, after exposure to hBN (0.8–400.0 μg/mL) for 24 and 72 h, HaCaT cells were washed thrice with PBS (200 μL/well), fixed for 1 h with 50 % trichloroacetic acid at 4 °C, and subsequently stained with 0.4 % SRB in 1 % acetic acid for 30 min. After washings with a 1 % acetic acid solution, the dye incorporated in each cell sample was dissolved in 10 mM TRIZMA base solution, and the absorbance was measured at 570 nm by the FLUOstar® Omega microplate reader (BMG LABTECH; Ortenberg, Germany). Data are presented as % of cell mass with respect to negative control (HaCaT cells not exposed to hBN).

2.12. Propidium iodide uptake assay

Necrotic cells were quantified measuring cells uptake of propidium iodide (PI). HaCaT cells exposed to hBN (0.8–400.0 μg/mL) for 24 and 72 h were washed thrice with PBS (200 μL/well) and incubated for 30 min at 37°C with 3 μM PI dissolved in PBS. Cells treated with 0.2 % Triton-X 100 were used as positive control. Fluorescence intensity was read by the FLUOstar® Omega microplate reader (BMG LABTECH; Ortenberg, Germany) with excitation and emission wavelengths of 485 nm and 590 nm, respectively. Samples were then permeabilized for additional 30 min with 0.2 % Triton-X to measure total fluorescence, as an index of total cell content. Data are reported as % of PI uptake as compared to positive control, after normalization on total cell content.

2.13. JC-1 mitochondrial depolarization assay

Mitochondrial depolarization in HaCaT cells was assessed by the JC-1 Mitochondrial Staining Kit (Sigma-Aldrich; Milan, Italy) according to the manufacturer's instructions. After exposure to hBN (0.8–400.0 μg/mL) for 24 and 72 h, cells were washed thrice with PBS (200 μL/well). Then, cells were incubated with 0.5 μM JC-1 (100 μL/well) for 20 min at

37 °C. After two washings with ice-cold culture medium, fluorescence was immediately quantified using the FLUOstar® Omega microplate reader (BMG LABTECH; Ortenberg, Germany). JC-1 aggregates (index of intact mitochondria) were detected with excitation and emission wavelengths of 530 nm and 590 nm, respectively; JC-1 monomers (index of disrupted mitochondria) were measured with a 485 nm and 570 nm filter combination. Results are expressed as a ratio between red and green fluorescence and are represented as % relative to negative control (HaCaT cells not exposed to hBN).

2.14. ATP detection assay

Intracellular ATP levels were quantified using the Luminescent ATP Detection Assay Kit (Abcam; Cambridge, UK), following the kit instructions. Briefly, after exposure to hBN (0.8–400.0 μg/mL) for 24 and 72 h, cells were washed thrice with PBS (200 μL/well) and treated with a detergent solution (50 μL/well) for 5 min on an orbital shaker. Afterwards, 50 μL/well of Substrate Solution were added. After 5 min on an orbital shaker in the dark, luminescence was detected by the FLUOstar® Omega microplate reader (BMG LABTECH; Ortenberg, Germany). Data are presented as % of intracellular ATP level with respect to negative control (HaCaT cells not exposed to hBN).

2.15. Dichlorofluorescin diacetate (DCFDA) assay

Reactive oxygen species (ROS) generated by HaCaT cells exposed to hBN were measured using the 2′,7′-dichlorofluorescin diacetate (DCFDA) fluorescence probe. After exposure to hBN (0.8–400.0 μg/mL) for 24 and 72 h, cells were washed thrice with PBS (200 μL/well). Then, cells were incubated with 100 μM DCFDA (100 μL/well) for 30 min at 37 °C, in the dark. After two washings with 200 μL/well of PBS containing Ca^{2+} and Mg^{2+}, fluorescence was read by the FLUOstar® Omega microplate reader (BMG LABTECH; Ortenberg, Germany), using an excitation and emission wavelengths combination of 485 nm and 570 nm. Results are presented as % of ROS production with respect to negative control (HaCaT cells not exposed to hBN).

2.16. SkinEthic™ reconstructed human epidermis model

SkinEthic™ Reconstructed human Epidermis (RhE), a commercial 3D epidermal tissue (EpiSkin; Lion, France) reconstructed from normal human keratinocytes, was used to assess corrosion and irritation potential of hBN. RhE was cultured on an inert polycarbonate filter at the air-liquid interface.

2.17. Skin corrosion evaluation

Skin corrosion potential of hBN was assessed on the SkinEthic™ RhE (0.5 cm^2, 17-day) following the OECD TG 431 [55]. Briefly, after RhE tissue equilibration period, tissue inserts were transferred onto fresh maintenance medium and topically exposed to powdered hBN (40 mg/cm^2) or 8 N potassium hydroxide (KOH; positive control) for 3 and 60 min at RT. Then, RhE tissue was washed 20 times with 1 mL PBS and subsequently incubated for 3 h with 1 mg/mL methylthiazolyldiphenyl-tetrazolium bromide (MTT) solution. Inserts were subsequently immersed in 1.5 mL isopropanol for 120 min under shaking at RT to extract formazan salts. RhE inserts were then perforated, and the formazan extract homogenized. Optical density (OD) was measured at 570 nm through the FLUOstar® Omega microplate reader (BMG LABTECH; Ortenberg, Germany). Data are expressed as % of RhE viability as compared to negative control (RhE not exposed to hBN). As a threshold given by the OECD TG 431, viabilities < 50 % after 3 min exposure or ≥ 50 % after 3 min exposure and < 15 % after 1 h exposure designate a corrosive substance.

2.18. Skin irritation evaluation

Skin irritation potential of hBN was assessed using the SkinEthic™ RhE according with the OECD TG 439 [56]. After RhE tissue equilibration period, tissue inserts were transferred onto fresh medium and topically exposed to powdered hBN (32 mg/cm^2) for 42 min at RT, or to 32 mg/cm^2 of the following compounds used as positive controls: sodium dodecyl sulphate (5 % SDS),1-chloro-2,4-dinitrobenzene (DNCB) or nickel sulfate ($NiSO_4$). RhE tissue was then rinsed 25 times with 1 mL PBS and subsequently incubated for 42 h. Then, tissues were incubated for 3 h with 1 mg/mL MTT solution. Inserts were subsequently immersed in 1.5 mL isopropanol for 120 min to extract formazan salts. RhE inserts were then perforated, and the formazan extract homogenized. OD was measured at 570 nm through the FLUOstar® Omega microplate reader (BMG LABTECH; Ortenberg, Germany). Data are expressed as % of RhE viability as compared to negative control (RhE not exposed to hBN). As stated in OECD TG 439, RhE viability ≤ 50 % defines an irritant substance.

2.19. Inflammatory mediators' release

To implement data on irritation potential, after RhE exposure to hBN (42 min) followed by 42 h post-treatment incubation, tissue media were collected and stored at −80°C. A number of inflammatory mediators [interleukin (IL)-1α, −1β, −6, −8, −7, −18, −33, tumor necrosis factor (TNF)-α, prostaglandin E_2 (PGE_2), and the chemokine regulated upon activation, normal T cell expressed and secreted (RANTES)], was quantified by commercial ELISA from Diaclone (Besançon, France) or Elabscience (Houston, TX, USA) according with the manufacturer's instructions. The amounts of inflammatory mediators in tissue media are expressed as pg/mL and results are the mean ± SE of three independent experiments performed in duplicate. Heatmap and clustering analysis were carried out to identify similar pattern of inflammatory mediators' release induced by the tested substances.

2.20. Statistical analysis

Data are expressed as the mean ± standard error (SE) from at least three independent experiments in triplicate. Results obtained in HaCaT cells were analyzed by two-way ANOVA analysis followed by Bonferroni's post-test (PrismGraphPad, Inc.; Boston, USA). One-way ANOVA followed by Bonferroni's post-test (PrismGraphPad, Inc.; Boston, USA) was used to analyzed results obtained from RhE tissues. Data were considered significant for p values lower than 0.05. Hierarchical clustering analysis of the inflammatory mediators' data and heatmap were obtained using the R Software (version 4.1.2).

3. Results and discussion

3.1. Physico-chemical characterization of hBN

Results on physico-chemical characterization of hBN are represented in Fig. 1. High-resolution transmission electron microscopy (HR-TEM) revealed flakes with a mean lateral size of 119.82 ± 55.58 nm, as determined from the size distribution analysis (Fig. 1, panels A, B). Raman spectroscopy (Fig. 1, panel C) showed a distinct peak at 1368.79 cm^{-1}, corresponding to the $E_{2\,g}$ vibrational mode, characteristic of the hexagonal structure of hBN [16]. The sharpness and position of this peak highlight the structural integrity and successful exfoliation of the material. Thermogravimetric analysis (TGA) performed under a nitrogen atmosphere demonstrated a residual weight loss of 1.6 wt% at 600°C (Fig. 1, panel D), that can be due to the presence of minimal oxygen functional groups. These findings corroborate the high thermal stability and purity of hBN, with no evidence of residual exfoliating agents [39,40].

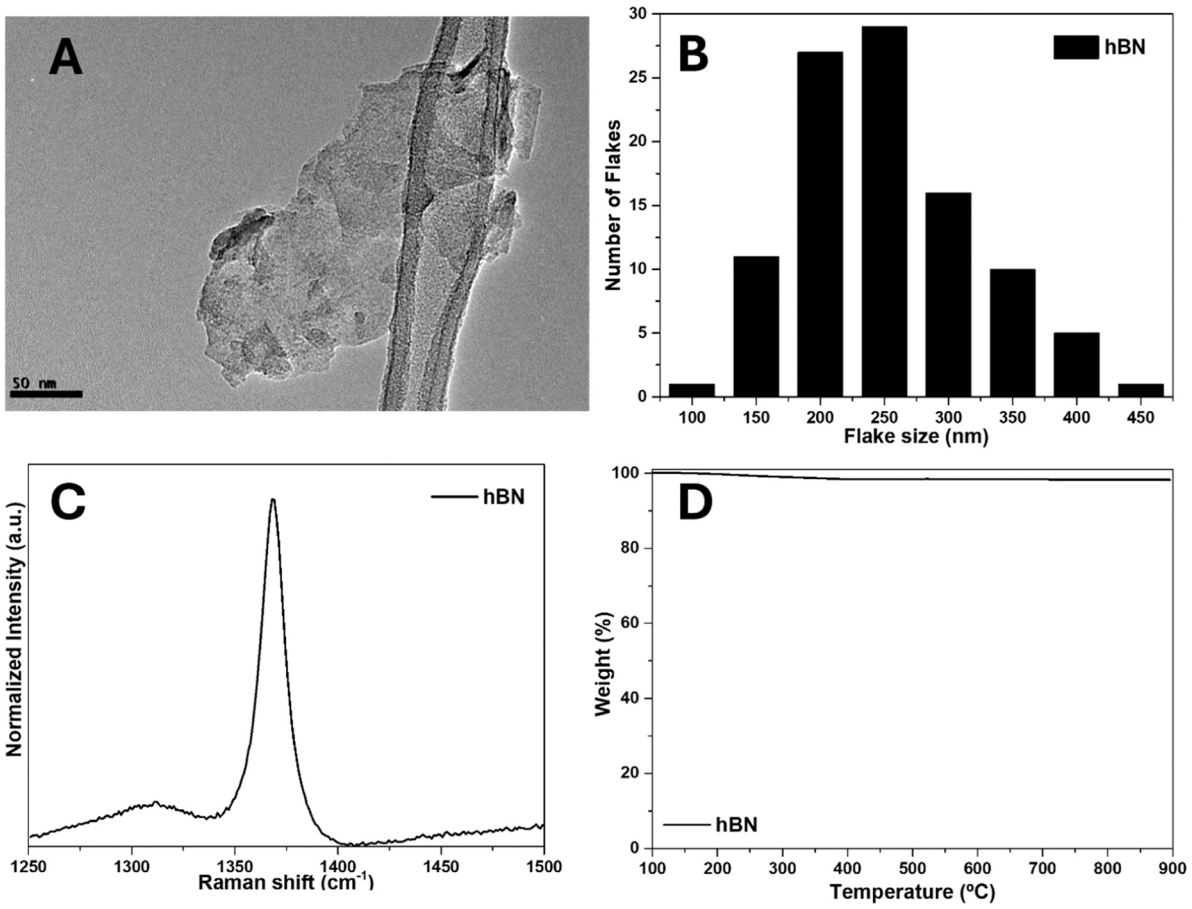

Fig. 1. A) Representative HR-TEM image showing hBN 2D material morphology; B) Lateral size distribution of the flakes derived from HR-TEM image analysis of hBN; C) Raman spectra highlighting the characteristic vibrational modes of hBN; D) TGA curve illustrating the thermal stability of hBN under a nitrogen atmosphere.

3.2. Detection of endotoxin

To exclude a possible hBN contamination by endotoxin, LAL chromogenic assay was initially performed. According to U.S. Food and Drug Administration (FDA), the endotoxin limit in medical devices for considering them not contaminated materials is 0.5 EU/mL [24]. As hBN showed a level of endotoxin equal to 0.39 EU/mL, below the threshold limit established by FDA (0.5 EU/mL), it can be considered non-contaminated by endotoxin (Table 1). However, considering that endotoxin quantitation by the conventional LAL assay could be tricky due to possible interference with some 2D nanomaterials [51], such possibility was ruled out spiking hBN (100 μg/mL) with 0.5 EU/mL endotoxin. LAL assay showed that endotoxin content in the endotoxin-spiked hBN sample (0.96 EU/mL) was comparable to the sum of endotoxin concentrations measured in hBN and the quantity of added endotoxin (0.91 EU/mL), suggesting lack of interferences (Table 1).

To further confirm the absence of endotoxin, a modified TET assay [61], originally set up for graphene-related materials to avoid interferences with the measurement [51], was performed using macrophages obtained from THP-1 cells differentiation. Cell media were collected from macrophages exposed for 24 h to a sub-cytotoxic concentration of hBN (12.5 μg/mL) with or without polymyxin B sulfate. Endotoxin content in hBN was extrapolated from a standard curve generated by LPS-induced TNF-α release by macrophages. Results, represented in Figure S1, are expressed as endotoxin units/mL (EU/mL) and demonstrated that endotoxin level in hBN was below the threshold of 0.5 EU/mL. In addition, the levels quantified in presence or absence of polymyxin B sulfate did not differ, confirming that hBN was not contaminated by endotoxin, as previously shown by the LAL assay.

Table 1
Endotoxin quantitation in hBN using LAL chromogenic assay. Endotoxin (E.coli O111:B4; 0.5 EU/mL) was included as control. U.S. FDA suggested acceptable limit for endotoxin: 0.5 EU/mL.

Sample	Concentration	Measured endotoxin [EU/mL] Mean ± SE
Endotoxin (*E.coli* O111:B4)	0.5 EU/mL	0.52 ± 0.02
hBN	100.0 μg/mL	0.39 ± 0.03
hBN + Endotoxin (*E.coli* O111:B4)	100.0 μg/mL + 0.5 EU/mL	0.96 ± 0.04

EU = endotoxin units.

3.3. Effects of hBN on HaCaT keratinocytes

3.3.1. Cellular internalization of hBN

Initially, hBN was investigated for its effects on human HaCaT skin keratinocytes, an *in vitro* model for cutaneous toxicity screening [30]. To evaluate hBN capability to interact with plasma membranes and to be internalized by keratinocytes, HaCaT cells exposed to hBN (50 μg/mL) for 24 and 72 h were analyzed by super-resolution SIM technique and, subsequently, by TEM. For SIM analysis, plasma membranes were labelled with red fluorescent DiL (Fig. 2, panel A) or F-actin filaments were stained with green fluorescent phalloidin (Fig. 2, panel B). In both cases, nuclei were labelled with Hoechst staining. Signals associated with the presence of hBN particles were acquired in bright field and colors were inverted off-line to allow their mapping at the cellular level. hBN particles were clearly able to interact with keratinocytes and to be internalized into cells. By merging the white signal given by hBN with

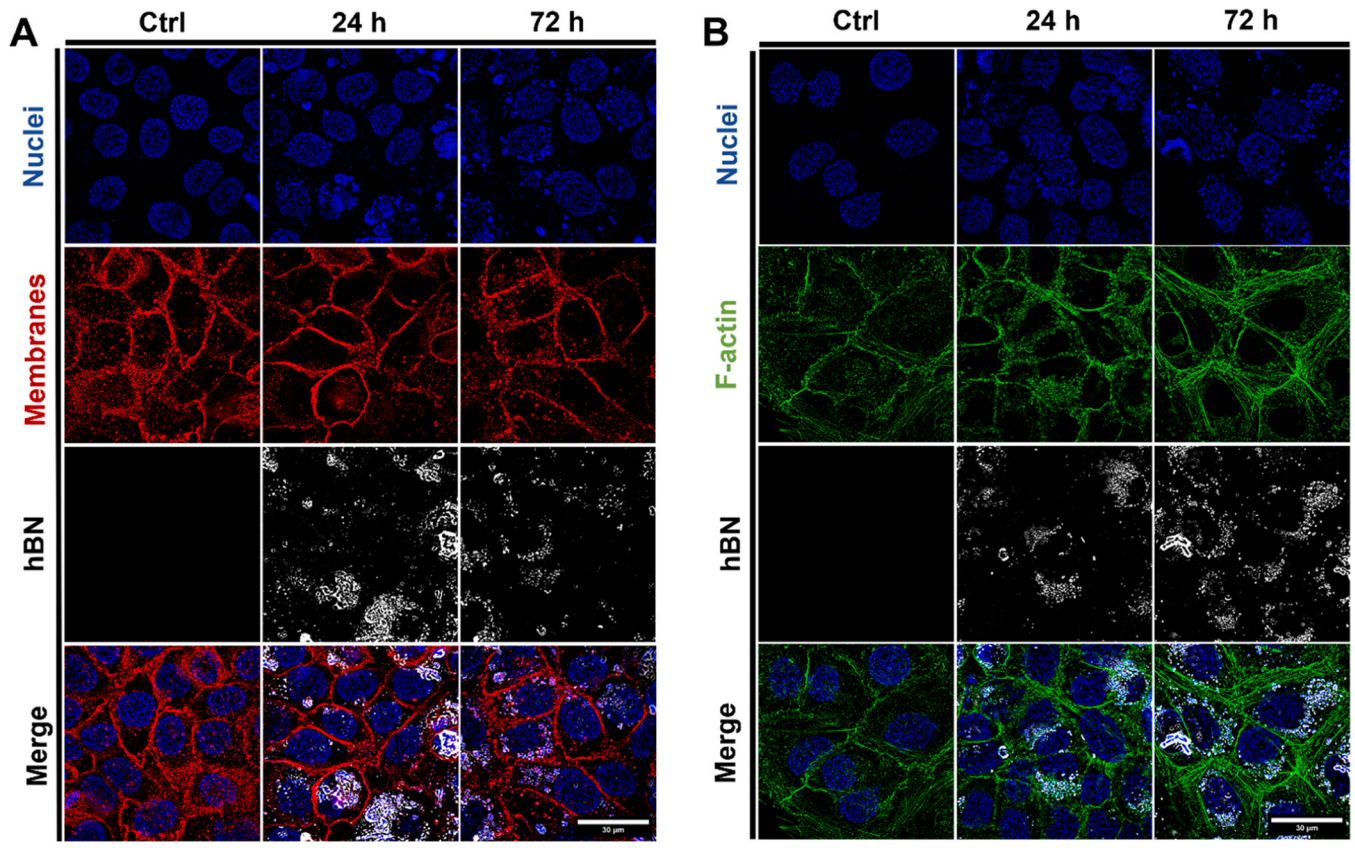

Fig. 2. Representative SIM images of HaCaT cells after exposure to hBN (50 μg/mL) for 24 or 72 h. Nuclei are labelled with Hoechst stain (blue); plasma membranes are labelled with the fluorescence dye DiL (red); F-actin filaments are labelled with fluorescence phalloidin (green); hBN particles are visualized in white (after colors inversion) and merged images represent the reconstruction of red/blue or green/blue labelled HaCaT cells merged with hBN particles' white signal. Magnification: 63X. Scale bar: 30 μm.

red/blue or green/blue fluorescence given by plasma membranes/nuclei or actin filaments/nuclei, respectively, hBN appeared to be partially associated with plasma membranes as well as dispersed into cytoplasm. Interestingly, hBN was clearly found inside cells, in particular around nuclei, suggesting massive penetration inside skin keratinocytes. However, despite this high internalization, morphological alterations in keratinocytes were not observed.

To confirm these findings, TEM analysis was performed, and relevant images are shown in Fig. 3. hBN particles were massively taken up by HaCaT cells already after 24 h exposure, confirming their localization around nuclei, but not inside them. After entering into HaCaT keratinocytes, hBN particles seemed also to be accumulated into lysosomes.

A recent study already reported hBN internalization by HaCaT keratinocytes after 24 h exposure at a slight lower concentration (20 μg/mL) [7]. Furthermore, our findings are supported also by a study exploiting forward scatter and side scatter in flow cytometry analysis demonstrating massive uptake of hBN nanosheets in human dermal fibroblast and human umbilical vein endothelial cells [70]. In addition, different theoretical studies demonstrated that, for hydrophobic nanoparticles, such as hBN, a direct interaction with the hydrophobic core of plasma membranes can promote cells internalization [13,41]; however, the uptake and the trafficking of nanomaterials strictly depend on their physico-chemical properties, such as surface chemistry, shape and especially size [66]. Moreover, using a combination of molecular dynamics simulations and *in vitro* tests on lung epithelial H460 cells, a recent study demonstrated lysosomal deposition of hBN sheets (with sharp and cornered morphology and polar edges) leading to intracellular consequences, such as lysosomal membrane permeabilization. The latter represents an emerging mechanism of cytotoxicity involving cathepsin B release and ROS production, ultimately triggering cell death [46].

3.4. Cytotoxic effects of hBN towards HaCaT cells

To assess cytotoxicity of hBN on HaCaT keratinocytes, different cellular parameters were evaluated: cell viability (WST-8 assay), cell mass (SRB assay) and integrity of plasma membrane (PI uptake assay). Then, three additional parameters were examined to investigate mitochondrial-related damages induced by hBN in HaCaT keratinocytes: mitochondrial membrane potential (JC-1 fluorescent assay), intracellular ATP levels (ATP detection assay) and ROS production (DCFDA fluorescent assay), which are the ones mostly affected by related 2D materials, such as graphene-related materials (GRMs), considered as reference [59,62]. Fig. 4 shows the effect of hBN (0.8–400 μg/mL) on these endpoints after 24 and 72 h exposure. WST-8 assay, widely exploited to investigate the effect of different 2D nanomaterials [59,76] on cell viability in terms of mitochondrial activity, was used to firstly assess hBN effect on keratinocytes. While no effects were observed after 24 h exposure, a significant reduction of cell viability down to 71 % ($p < 0.01$) was recorded after 72 h exposure to hBN concentrations equal or higher than 100 μg/mL (Fig. 4, panel A). Thus, the relatively low cytotoxic effect of hBN, not allowing the computation of EC_{50} values, suggests its good biocompatibility with HaCaT cells. Subsequently, the low hBN cytotoxicity was confirmed in terms of cell mass, evaluated by the SRB assay. Compared to WST-8 assay, hBN cytotoxic potency was slightly enhanced only after 72 h exposure, when the material provoked a significant concentration-dependent decrease of cell mass at concentrations ranging from 100 to 400 μg/mL (57–44 % of cell mass, respectively; $p < 0.001$) (Fig. 4, panel B). Then, PI uptake assay was carried out to verify if these effects could be related to a plasma membrane damage. After 24 h exposure, hBN caused a weak, but significant, increase of PI uptake only at the highest concentrations (19 %

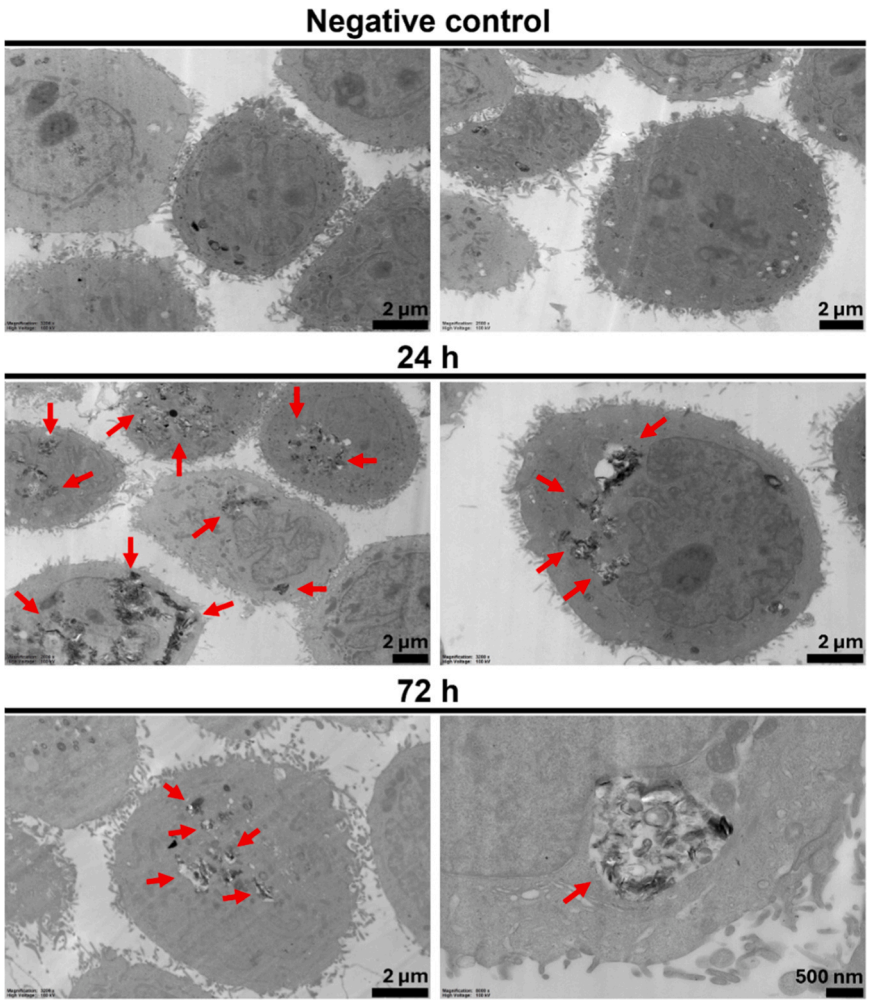

Fig. 3. Representative TEM images of HaCaT cells after exposure to hBN (50 µg/mL) for 24 or 72 h. Red arrows indicate particles inside the cells.

and 24 % at 200 and 400 µg/mL, respectively; $p < 0.05$). On the contrary, a pronounced concentration-related increase of PI uptake occurred after 72 h exposure to the concentration of 25 µg/mL (20 %; $p < 0.05$) and above (up to 65 % at400 µg/mL; $p < 0.0001$) (Fig. 4, panel C).

Altogether, these observations lead to hypothesize that HaCaT cells exposure to very high hBN concentrations, mainly for 72 h, could allow a material interaction with plasma membrane, impairing its integrity and cell viability. Our findings are in accordance with those of previous studies on hBN nanoparticles, demonstrating slight cytotoxic effects on fibroblasts and keratinocytes only after exposure to high concentrations (>80 µg/mL) for 24 h [1,18,38,50], even though these findings were recorded by other cytotoxicity assays (i.e., lactate dehydrogenase cell release). Intriguingly, these effects seem to be exerted by hBN with a potency lower than that of some GRMs, previously studied using the same cell model with the same experimental settings. Indeed, few layers graphene (FLG) and graphene oxide (GO) induced a significant cellular damage already at lower concentrations (>30 µg/mL and >1 µg/mL for FLG and GO, respectively), and their potency was influenced by the oxidation state [59].

Regarding mitochondrial-related cytotoxic effects, mitochondrial depolarization was assessed in HaCaT cells exposed to hBN for 24 and 72 h by JC-1 fluorescent assay. JC-1 is a fluorescent probe accumulated in functional mitochondria due to the polarized mitochondrial membrane. Any event that dissipates mitochondrial membrane potential, such as mitochondrial membrane disruption, avoids this accumulation, determining a shift in JC-1 fluorescence. As reported in Fig. 4 (panel D), already after 24 h treatment, hBN (0.8–100 µg/mL) caused a concentration-dependent increase of mitochondrial membrane depolarization (38 % at 100 µg/mL; $p < 0.001$). After 72 h, the highest concentration tested (100 µg/mL) increased mitochondrial depolarization by 44 % ($p < 0.001$). Concentrations of hBN higher than 100 µg/mL were excluded from the analysis due to interferences between hBN and the reagents used.

Subsequently, intracellular levels of ATP were detected through a luminescence assay to assess if HaCaT cells exposure to hBN could affect mitochondrial energy metabolism. Already after 24 h, hBN provoked a weak, but significant, reduction of ATP production at the concentrations of 200 µg/mL (78 % of ATP production; $p < 0.01$) and 400 µg/mL (74 % of ATP production; $p < 0.001$). Prolonging cells exposure to 72 h, hBN determined a concentration-dependent drop in ATP levels at the concentration of 50 µg/mL (75 % of ATP production; $p < 0.001$) and above, with maximum effect at 400 µg/mL (19 % of ATP production; $p < 0.0001$) (Fig. 4, panel E). These results suggest that hBN can significantly alter mitochondrial membrane potential as a possible mechanism of mitochondrial damage in terms of impaired energy metabolism and mitochondrial activity, albeit only at high concentrations. These observations are in accordance with previous findings showing hBN ability to induce mitochondrial depolarization in different cell types [44,70].

Lastly, given the strong correlation between mitochondrial disfunction and ROS generation, hBN ability to evoke oxidative stress in keratinocytes was measured by the DCFDA assay. As compared to negative control, 24 and 72 h treatment with 50 µg/mL hBN significantly

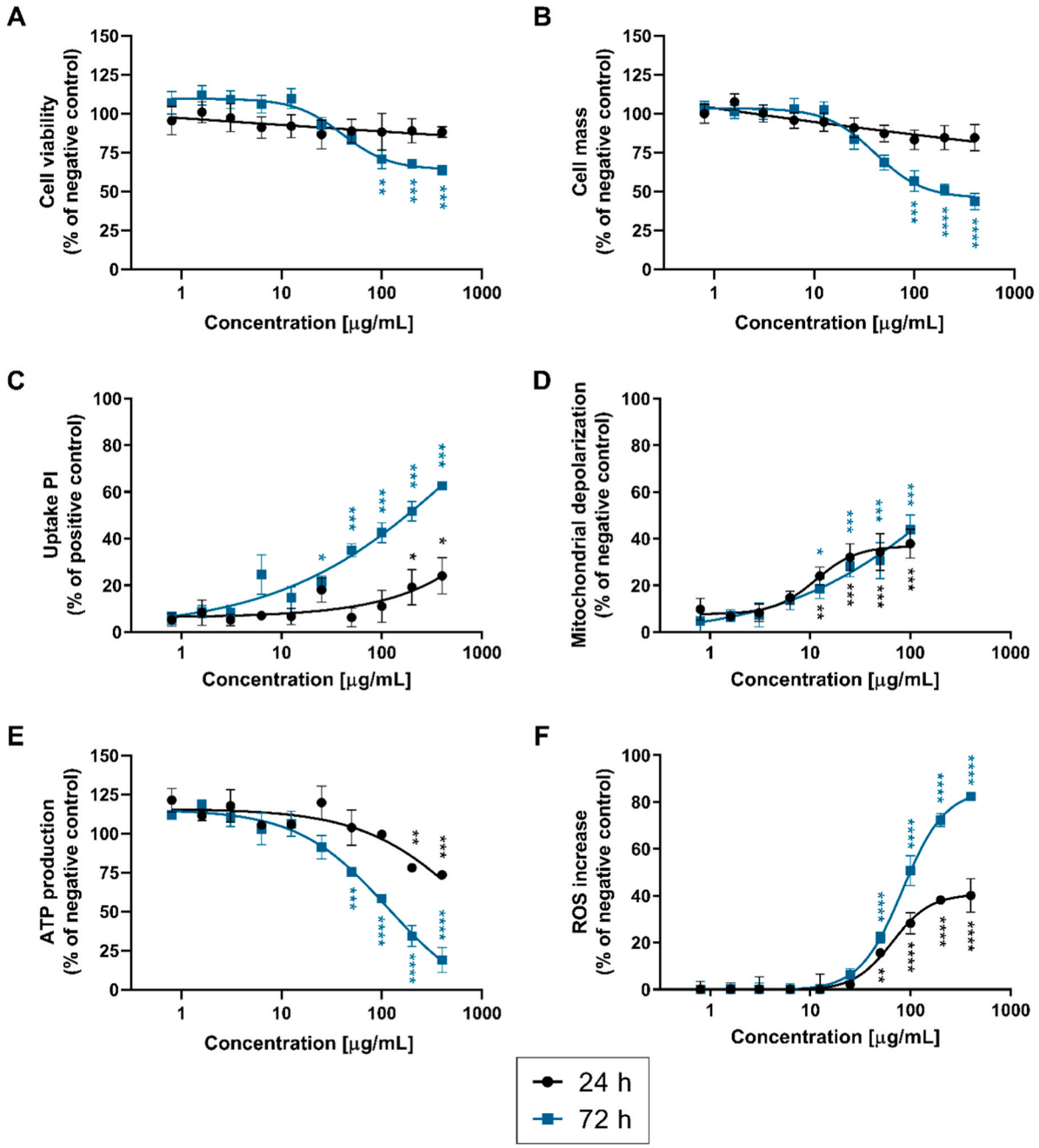

Fig. 4. Effects of hBN (0.8–400.0 µg/mL) on cell viability (WST-assay, panel A), cell mass (SRB assay, panel B), plasma membrane integrity (uptake of PI assay, panel C), mitochondrial depolarization (JC-1 fluorescent assay, panel D), ATP production (ATP detection assay, panel E), and ROS production (DFCDA assay, panel F) in HaCaT cells. Data are the mean ± SE of at least three independent experiments carried out in triplicate. Statistical differences vs negative controls: * , $p < 0.05$; * *, $p < 0.01$; * ** , $p < 0.001$; * ** *, $p < 0.0001$ (Two-way ANOVA and Bonferroni's post test).

increased ROS levels by 16 % ($p < 0.01$) and 22 % ($p < 0.0001$), respectively. The highest concentration (400 µg/mL) induced 40 % ($p < 0.0001$) and 82 % ($p < 0.0001$) increase, respectively (Fig. 4, panel F). These findings are in agreement with those of a previous study on mHippo E-14 cells, showing a significant ROS production induced by hBN at the concentration of 44 µg/mL, both after 24 and 72 h exposure [75]. On the contrary, Şen and colleagues pointed out, not only the inability of hBN to induce ROS production, but also its capability to inhibit ROS generation at a high concentration (100 µg/mL) in human dermal fibroblasts and human umbilical vein endothelial cells [70]. However, these differences could be tentatively ascribed to diverse methods of hBNs production or to other hBNs features, such as their size and shape.

On the whole, our results suggest that mitochondrial dysfunction (mitochondrial depolarization and impairment of energy metabolism) and oxidative stress could represent key events involved in hBN cytotoxicity towards keratinocytes. In particular, hBN seems to induce ROS production at concentrations higher than those inducing mitochondrial depolarization and perturbation of energy metabolism, suggesting that oxidative stress might be a consequence, and not the cause, of mitochondrial dysfunction. However, it has be considered that also these parameters were affected by high hBN concentrations as compared to those of GRMs (Pelin et al., 2018b), highlighting, once again, a high biocompatibility of hBN.

With the attempt to elucidate the role of mitochondria in the mechanism of hBN cytotoxicity, a set of experiments was carried out in

presence of cyclosporine-a (CyclA), inhibitor of mitochondrial permeability transition pore (MPTP) formation [54], or N-acetyl-cysteine (NAC), an anti-oxidant able to protect mitochondria by reducing ROS-dependent mitochondrial depolarization [48,72]. HaCaT cells were pre-exposed to 0.2 μM CyclA or 1 mM NAC for 1 h before exposure to hBN (12.5–100.0 μg/mL) and CyclA or NAC for 72 h. Results showed in Supplementary Figure S2 demonstrate that both CyclA and NAC slightly, but significantly, inhibited mitochondrial depolarization induced by hBN, but they did not influence the reduced cell viability. This observation suggests that: *i*) mitochondrial depolarization is only partially caused by a biochemically-modulated response, such as opening of MPTP, and *ii*) the inhibition of this phenomenon, only in a minor part responsible of mitochondrial dysfunction, is not sufficient to restore cell viability. On the whole, these data suggest that the reduced cell viability and the related mitochondrial depolarization induced by hBN are not primarily associated to a biochemically-controlled response, but could be rather ascribed to a physical damage at the plasma and mitochondrial membranes levels. Indeed, a recent study on neonatal human dermal fibroblasts demonstrated that low concentrations of BN nanosheets spontaneously penetrated mitochondrial lipid membranes through hydrophobic interactions. Once penetrated, BN induced heterogeneous lipid packing and mitochondrial fragmentation, determining morphological and functional alterations of mitochondria. These alterations activated cell autophagy as clearance mechanism to remove damaged mitochondria and maintain cell viability [64]. It should be underlined that results showed in Figs. 2 and 3 clearly demonstrate hBN internalization into cells, therefore supporting the hypothesis of a direct physical damage to mitochondria.

3.5. Effects of hBN on 3D reconstructed human epidermis

3.5.1. Skin corrosion and irritation

It should be noted that, despite their functional and biochemical relevance, common *in vitro* 2D epidermal cell cultures do not completely resemble the intact epidermis morphology. Thus, 3D models of epidermis enable the formation of intercellular junctions, the maintenance of tissue integrity and barrier function, making them more reliable and predictive [34]. In this study, we used the SkinEthic™ Reconstructed human Epidermis (RhE), a standardized commercially-available 3D model of epidermis, constituted by non-transformed human keratinocytes, closely simulating histological, biochemical, physiological and morphological properties of epidermis [53]. We focused on the assessment of two main adverse effects at the cutaneous level (corrosion and irritation), adopting two specific TGs defined by the OECD (431 and 439, respectively) [55,56]. OECD TGs define commonly accepted procedures that should be strictly followed to assess different adverse outcomes that must be considered for all substances that should be commercialized, to collect toxicological data suitable for international regulatory requirements [22]. In fact, they have been included in New Approach Methodologies, as alternative non-animal methods useful for the hazard characterization and risk assessment of substances, in compliance with the 3 R's principles (replacement, reduction and refinement) [57].

However, it should be noted that no OECD standards predicting skin adverse outcomes of 2D nanomaterials are currently available, and most TGs, originally validated for chemicals, need to be adapted to this particular category [5]. Recently, we carefully demonstrated the possibility to adopt TG 431 and 439 also for 2D GRMs without introducing any modifications to the protocol [6,28]. Given the similarities between GRMs and hBN in terms of physico-chemical behavior, the same assumptions could be made also for testing other 2D materials, such as hBN. The protocols described in the OECD TGs 431 and 439 are similar not only for the model (3D RhE), but also for the readout used for the prediction: skin corrosion and irritation potentials are assessed by means of reduced tissue viability after treatment with the test substances, using the MTT assay.

On these grounds, we firstly evaluated skin corrosion properties of powdered hBN (40 mg/cm^2). As reported in Fig. 5 (panel A), 3 min or 1 h exposure to hBN did not significantly reduce RhE viability with respect to untreated controls. Being below the thresholds defined by the OECD TG 431 (tissue viability <50 % after 3 min exposure or <15 % after 1 h exposure), the negligible reduction of tissue viability induced by hBN suggests that the material can be considered as non-corrosive. As expected, 3 min exposure to the positive control (8 N KOH) significantly decreased tissue viability to 0.7 % ($p < 0.0001$), confirming that it is a corrosive substance, belonging to the Sub-category 1 A of the United Nations Globally Harmonized System of Classification and Labelling of Chemicals (UN GHS) [78].

However, a substance identified as non-corrosive should be tested also for its potential as skin irritant. Such property refers to the ability of a topically applied substance to induce a reversible skin damage, typically correlated with the development of an inflammatory reaction. As shown in Fig. 5 (panel B), hBN (32 mg/cm^2) turned out to be non-irritant, since RhE viability reduction was below the threshold given by the OECD TG 439 (tissue viability: ≤50 %) after 42 min exposure followed by 42 h post-treatment incubation. In contrast, the positive control (5 % SDS) decreased tissue viability to 1.1 %, demonstrating its irritant properties ($p < 0.0001$). Moreover, two other chemicals were included into this analysis, DNCB and $NiSO_4$ (32 mg/cm^2), as reference agents, the first inducing both irritation and sensitizing effects, the second one being a skin sensitizer. These additional reference controls were added to subsequently investigate if the pattern of pro-inflammatory mediators released by hBN-treated RhE was comparable to an irritant (SDS) or a sensitizing agent (DNCB, $NiSO_4$), given the involvement of an inflammatory reaction in both adverse outcomes. In detail, DNCB induced a considerable reduction of RhE viability to 1 % ($p < 0.0001$), confirming its irritant properties, besides its sensitizing ones. $NiSO_4$ significantly decreased tissue viability to 72 % ($p < 0.0001$), above the threshold level predicting an irritant effect, indicating its slight toxicity towards RhE tissue, without skin irritant properties.

3.6. Pro-inflammatory effects of hBN

Inflammatory mediators quantitation is useful for an improved assessment of skin irritant properties, since even sub-cytotoxic concentrations of a substance could activate inflammatory processes and also immune stress [58]. To assess the inflammation state of RhE and to implement the data obtained adopting the OECD TG 439, tissue media from treated RhE tissues were collected to quantify a panel of selected pro-inflammatory mediators (IL-1α, −1β, −6, −7, −8, −18, −33, TNF-α, PGE_2 and RANTES) and to assess hBN ability to stimulate epidermal keratinocytes as initiators of a possible skin inflammation. Figure S3 shows the concentrations of each inflammatory mediator (pg/mL) measured in culture media after RhE exposure to hBN, DNCB, $NiSO_4$ (32 mg/cm^2) or 5 % SDS (positive control), in comparison with that recorded in RhE exposed to PBS (negative control). In general, inflammatory mediators' release pattern induced by hBN seems to be comparable to that of negative control, suggesting the lack of pro-inflammatory potential, in accordance with the absence of irritation. Slight, but significant, alterations in the release of IL-1α, −8, −18, −33, PGE_2 and RANTES were found only for DNCB, $NiSO_4$ or the positive control SDS.

With respect to negative control (IL-1α = 49 pg/mL; Fig. S3, panel A), a significant increase in the release of IL-1α, a useful marker for the discrimination between irritant and non-irritant substances [10], was found only for the positive control 5 % SDS (342 pg/mL, equal to a 8.1-fold increase; $p < 0.0001$), confirming previously findings [37,47,63,74]. In addition, with respect to negative controls (IL-8 = 65 pg/mL; IL-33: 30.0 pg/mL), only the positive control SDS, but not the sensitizing substances, determined a mild, but significant, increase in the release of IL-8 (80 pg/mL, equal to a 1.2-fold increase; $p < 0.01$; Fig. S3, panel E) and IL-33 (36 pg/mL, equal to a 1.2-fold increase; $p < 0.01$; Fig. S3,

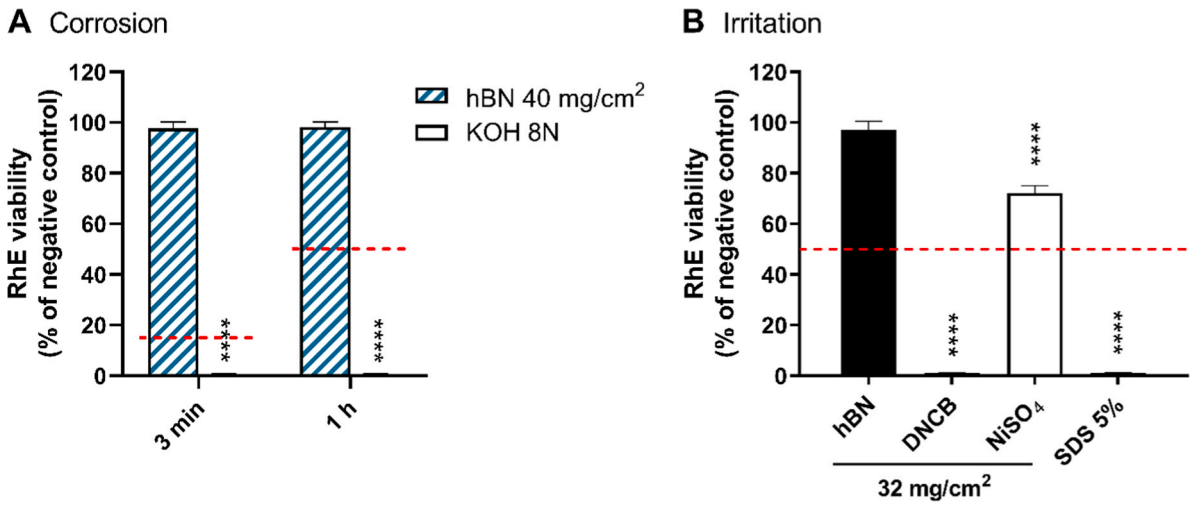

Fig. 5. Skin corrosion (panel A) and irritation (panel B) properties of hBN, controls and reference substances evaluated as SkinEthic™ Reconstructed Human Epidermis (RhE) viability. Results are the mean ± SE of three independent experiments. Corrosion was predicted on the basis of the relevant thresholds given by the OECD TG 431 (panel A, dashed red lines), while irritation was predicted on the basis of the threshold given by the OECD TG 439 (panel B, dashed red line). Statistical differences vs negative controls: * ** *, $p < 0.0001$ (One-way ANOVA and Bonferroni's post-test).

panel G). IL-8 is a chemotactic factor for neutrophils and T lymphocytes [4], while IL-33 is a mediator able to drive the T-helper type 2 cells responses acting as an alarmin [29]. The lack of IL-8 release by RhE tissues exposed to sensitizing DNCB and $NiSO_4$ is not in line with the findings by other studies reported in literature [9,27]. However, the discrepancy in the results could be due to the short-term treatment of RhE (42 min) if compared to the treatments with sensitizers reported in other studies (up to 24 h).

On the contrary, in comparison to negative control (IL-18 = 15 pg/mL; Fig. S3, panel F), only DNCB and $NiSO_4$ determined a weak but significant increase of IL-18 release to 16 pg/mL for both substances (1.1-fold increase; $p < 0.01$). IL-18 could be used to discriminate sensitizers from irritants [2,11]; since hBN did not induce IL-18 release, in contrast to DNCB and $NiSO_4$ that slightly increased its release, this result supports the hypothesis that hBN is not a skin sensitizer. However, our findings using 3D RhE do not rule out a possible involvement of the immune system to exclude sensitizing potential of hBN. Nonetheless, a previous study reported extremely low irritant and sensitizing properties for boron nitride in different cosmetic formulations, assessed through human occlusive and/or repeated insult patch tests [26].

Regarding PGE_2, a mediator able to regulate lymphocyte functions [36], only DNCB induced its significant increase to 28 pg/mL (1.2-fold; $p < 0.05$), as compared to negative control (23 pg/mL; Fig. S3, panel I). Lastly, "regulated upon activation normal T expressed and secreted" (RANTES) is a selective chemoattractant factor for monocytes and lymphocytes during early stages of inflammation in keratinocytes [68]. As shown in Figure S3 (panel J), both DNCB and the positive control (5 % SDS) induced a significant reduction of RANTES release to 504 pg/mL (23.2-fold decrease; $p < 0.05$) and 3015 pg/mL (3.7-fold decrease; $p < 0.05$), respectively, in comparison with that induced by negative control (11219 pg/mL). On the contrary, none of the tested substances increased the release of IL-1β (Fig. S3, panel B), IL-6 (Fig. S3, panel C), IL-7 (Fig. S3, panel D) and TNF-α (Fig. S3, panel H).

Altogether, these data suggest the lack of pro-inflammatory potential for hBN, given the low amounts of released inflammatory mediators measured. To confirm this observation, associations among the pattern of inflammatory mediators' release for each tested substance were evaluated by a hierarchical cluster analysis, as represented in Fig. 6. The analysis showed one major cluster comprising hBN, negative control and $NiSO_4$, suggesting a comparable mediators' release pattern, supporting the results obtained adopting the OECD TG 439 and suggesting a negligible pro-inflammatory potential of hBN after 42 min exposure

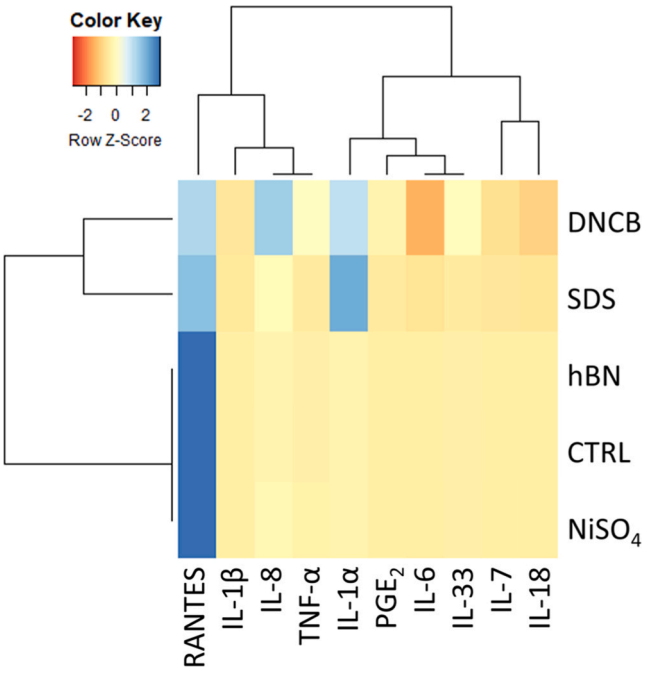

Fig. 6. Heatmap and relevant hierarchical cluster analysis made on inflammatory mediators data, released by RhE exposed to hBN, $NiSO_4$ and DNCB (32 mg/cm^2) and the positive control for irritation SDS (5 %) for 42 min, followed by 42 h of post-treatment incubation. Similarity among samples is depicted by each branch of the dendrograms, shorter branches representing more comparable patterns.

followed by 42 h of post-treatment incubation. Intriguingly, the sensitizer, albeit not irritant, $NiSO_4$, grouped together with this cluster, suggesting an extremely low pro-inflammatory potential despite its sensitization properties, considering this specific panel of inflammatory mediators. On the other hand, inflammatory mediators release induced by the irritant and strong sensitizer DNCB and the positive control SDS were not grouped in a specific primary cluster, suggesting different release patterns.

4. Conclusions

Overall, the present *in vitro* study contributes to elucidate hBN toxic potential at the cutaneous level. In particular, despite its significant uptake into keratinocytes, hBN exerted only weak cytotoxic effects. Only slight alterations in viability, mass and plasma membrane integrity of HaCaT cells were recorded at high concentrations (>25 μg/mL), mainly after 72 h exposure. Moreover, in the effort to explore the mechanism underlying its cutaneous toxicity, even if low, hBN was evaluated for its ability to alter a series of cellular parameters known to be affected in the same cell model by 2D GRMs, considered as referenced 2D materials. In particular, the decreased cell viability and the disruption of plasma membrane integrity appeared associated with a mitochondrial damage causing secondary ROS production and drop of ATP intracellular level; however, these effects appear to be induced at hBN concentrations higher than those previously reported for different GRMs, suggesting a higher hBN biocompatibility with keratinocytes.

In addition, skin biocompatibility was further evaluated on the 3D RhE model, through the adoption of the OECD TG 431 and 439 to assess skin corrosion and irritation properties of hBN, respectively. No major limitations for the adoption of these TGs (originally validated for chemicals) to hBN were noticed, in line with the same observation previously made for GRMs. Their adoption allowed us to collect robust and reliable data demonstrating hBN as a non-corrosive and non-irritant material and with an extremely low pro-inflammatory potential.

Altogether, these results represent a significant gain on knowledge about the hazard characterization of hBN at the skin level. However, future studies will be necessary to investigate the role of key hBN physico-chemical properties in its toxic potential at the skin level, in line with the Safe-by-Design principle, as well as to study long-term effects. Anyway, these data acquire a particular interest for the safe use of hBN-enriched technological applications directly in contact with the skin and/or for workers involved in hBN manufacturing.

Environmental implication

Beside graphene, only limited information is available about the safety profile of other 2D materials, such as hexagonal boron nitride (hBN). Given the potential release of hBN into the environment during its whole life-cycle, the risk for the environment, as well as for human health, could not be excluded. Hence, this study provides robust toxicological data characterizing the hazard posed by hBN, considering skin contact as one of the most important exposure routes to this material once released in the environment as well as in an occupational scenario.

CRediT authorship contribution statement

Carlin Michela: Writing – original draft, Investigation, Formal analysis, Data curation. **Sosa Silvio:** Writing – review & editing, Data curation. **González Viviana Jehová:** Resources, Investigation. **Tubaro Aurelia:** Writing – review & editing. **Pelin Marco:** Writing – review & editing, Supervision, Funding acquisition, Data curation, Conceptualization. **Vázquez Ester:** Writing – review & editing, Resources. **Prato Maurizio:** Writing – review & editing, Supervision, Funding acquisition.

Declaration of Competing Interest

The authors declare that they have no known competing financial interests or personal relationships that could have appeared to influence the work reported in this paper

Acknowledgements

This study was financially supported by the European Commission Graphene Flagship Core 3 (grant agreement no. 881603). Part of this study was financed by the Italian National Institute for Insurance against Accidents at Work (INAIL) in the frame of the SAF€RA 2022 program (Safe2energy project).

Graphics for Table of Contents were created using Biorender.

Appendix A. Supporting information

Supplementary data associated with this article can be found in the online version at doi:10.1016/j.jhazmat.2025.138449.

Data availability

Data will be made available on request.

References

[1] Abdelnasir, S., Mungroo, M.R., Shahabuddin, S., Siddiqui, R., Khan, N.A., Anwar, A., 2021. Polyaniline-conjugated boron nitride nanoparticles exhibiting potent effects against pathogenic brain-eating amoebae. ACS Chem Neurosci 12 (19), 3579–3587. https://doi.org/10.1021/acschemneuro.1c00179.

[2] Andres, E., Barry, M., Hundt, A., Dini, C., Corsini, E., Gibbs, S., Roggen, E.L., Ferret, P.-J., 2017. Preliminary performance data of the RHE/IL-18 assay performed on SkinEthic™ RHE for the identification of contact sensitizers. Int J Cosmet Sci 39 (2), 121–132. https://doi.org/10.1111/ics.12355.

[3] Ares, P., Cea, T., Holwill, M., Wang, Y.B., Roldán, R., Guinea, F., Andreeva, D.V., Fumagalli, L., Novoselov, K.S., Woods, C.R., 2020. Piezoelectricity in monolayer hexagonal boron nitride. Adv Mater 32 (1), 1905504. https://doi.org/10.1002/adma.201905504.

[4] Barker, J.N.W.N., Griffiths, C.E.M., Nickoloff, B.J., Mitra, R.S., Dixit, V.M., Nickoloff, B.J., 1991. Keratinocytes as initiators of inflammation. Lancet 337 (8735), 211–214. https://doi.org/10.1016/0140-6736(91)92168-2.

[5] Bleeker, E.A.J., Swart, E., Braakhuis, H., Fernández Cruz, M.L., Friedrichs, S., Gosens, I., Herzberg, F., Jensen, K.A., von der Kammer, F., Kettelarij, J.A.B., Navas, J.M., Rasmussen, K., Schwirn, K., Visser, M., 2023. Towards harmonisation of testing of nanomaterials for EU regulatory requirements on chemical safety – A proposal for further actions. Regul Toxicol Pharmacol 139, 105360. https://doi.org/10.1016/j.yrtph.2023.105360.

[6] Carlin, M., Garrido, M., Sosa, S., Tubaro, A., Prato, M., Pelin, M., 2023. In vitro assessment of skin irritation and corrosion properties of graphene-related materials on a 3D epidermis. Nanoscale 15 (35), 14423–14438. https://doi.org/10.1039/D3NR03081D.

[7] Carlin, M., Kaur, J., Ciobanu, D.Z., Song, Z., Olsson, M., Totu, T., Gupta, G., Peng, G., González, V.J., Janica, I., Pozo, V.F., Chortarea, S., Buljan, M., Buerki-Thurnherr, T., Rio Castillo, A.E.D., Thorat, S.B., Bonaccorso, F., Tubaro, A., Vazquez, E., Pelin, M., 2024. Hazard assessment of hexagonal boron nitride and hexagonal boron nitride reinforced thermoplastic polyurethane composites using human skin and lung cells. J Hazard Mater 473, 134686. https://doi.org/10.1016/j.jhazmat.2024.134686.

[8] Cassabois, G., Valvin, P., Gil, B., 2016. Hexagonal boron nitride is an indirect bandgap semiconductor. Article 4. Nat Photonics 10 (4). https://doi.org/10.1038/nphoton.2015.277.

[9] Coquette, A., Berna, N., Vandenbosch, A., Rosdy, M., De Wever, B., Poumay, Y., 2003. Analysis of interleukin-1alpha (IL-1alpha) and interleukin-8 (IL-8) expression and release in in vitro reconstructed human epidermis for the prediction of in vivo skin irritation and/or sensitization. Toxicol Vitr: Int J Publ Assoc BIBRA 17 (3), 311–321. https://doi.org/10.1016/s0887-2333(03)00019-5.

[10] Corsini, E., Galli, C.L., 1998. Cytokines and irritant contact dermatitis. Toxicol Lett 102–103, 277–282. https://doi.org/10.1016/s0378-4274(98)00323-3.

[11] Corsini, E., Mitjans, M., Galbiati, V., Lucchi, L., Galli, C.L., Marinovich, M., 2009. Use of IL-18 production in a human keratinocyte cell line to discriminate contact sensitizers from irritants and low molecular weight respiratory allergens. Toxicol Vitr: Int J Publ Assoc BIBRA 23 (5), 789–796. https://doi.org/10.1016/j.tiv.2009.04.005.

[12] Cun, H., Miao, Z., Hemmi, A., Al-Hamdani, Y., Iannuzzi, M., Osterwalder, J., Altman, M.S., Greber, T., 2021. High-quality hexagonal boron nitride from 2D distillation. ACS Nano 15 (1), 1351–1357. https://doi.org/10.1021/acsnano.0c08616.

[13] Curtis, E.M., Bahrami, A.H., Weikl, T.R., Hall, C.K., 2015. Modeling nanoparticle wrapping or translocation in bilayer membranes. Nanoscale 7 (34), 14505–14514. https://doi.org/10.1039/c5nr02255j.

[14] da Silva, W.M., de Andrade Alves e Silva, R.H., Cipreste, M.F., Andrade, G.F., Gastelois, P.L., de Almeida Macedo, W.A., de Sousa, E.M.B., 2020. Boron nitride nanotubes radiolabeled with 153Sm and 159Gd: potential application in nanomedicine. Appl Radiat Isot 157, 109032. https://doi.org/10.1016/j.apradiso.2019.109032.

[15] De Pasquale, D., Marino, A., Tapeinos, C., Pucci, C., Rocchiccioli, S., Michelucci, E., Finamore, F., McDonnell, L., Scarpellini, A., Lauciello, S., Prato, M., Larrañaga, A., Drago, F., Ciofani, G., 2020. Homotypic targeting and drug delivery in glioblastoma cells through cell membrane-coated boron nitride nanotubes. Mater Des 192, 108742. https://doi.org/10.1016/j.matdes.2020.108742.

[16] de Souza, R.F.B., Maia, V.A., Zambiazzi, Priscilla, J., Otubo, L., Lazar, D.R.R., Neto, A.O., 2021. Facile, clean and rapid exfoliation of boron-nitride using a non-

thermal plasma process. Mater Today Adv 12, 100181. https://doi.org/10.1016/j.mtadv.2021.100181.
[17] Deepika, Li, L.H., Glushenkov, A.M., Hait, S.K., Hodgson, P., Chen, Y., 2014. High-efficient production of boron nitride nanosheets via an optimized ball milling process for lubrication in oil. Sci Rep 4, 7288. https://doi.org/10.1038/srep07288.
[18] Deshmukh, A.R., Chaturvedi, P.K., Lee, S.-Y., Park, W.-Y., Kim, B.S., 2022. One-step green production of biocompatible functionalized few-layer graphene/boron nitride nanosheet hybrids using tannic acid-based liquid-phase exfoliation. ACS Sustain Chem Eng 10 (29), 9573–9583. https://doi.org/10.1021/acssuschemeng.2c02484.
[19] Díez-Pascual, A.M., Díez-Vicente, A.L., 2016. PEGylated boron nitride nanotube-reinforced poly(propylene fumarate) nanocomposite biomaterials. RSC Adv 6 (83), 79507–79519. https://doi.org/10.1039/C6RA09884C.
[20] Emanet, M., Kazanç, E., Çobandede, Z., Çulha, M., 2016. Boron nitride nanotubes enhance properties of chitosan-based scaffolds. Carbohydr Polym 151, 313–320. https://doi.org/10.1016/j.carbpol.2016.05.074.
[21] Emanet, M., Şen, Ö., Çobandede, Z., Çulha, M., 2015. Interaction of carbohydrate modified boron nitride nanotubes with living cells. Colloids Surf B: Biointerfaces 134, 440–446. https://doi.org/10.1016/j.colsurfb.2015.07.036.
[22] Eskes, C., Detappe, V., Koëter, H., Kreysa, J., Liebsch, M., Zuang, V., Amcoff, P., Barroso, J., Cotovio, J., Guest, R., Hermann, M., Hoffmann, S., Masson, P., Alépée, N., Arce, L.A., Brüschweiler, B., Catone, T., Cihak, R., Clouzeau, J., Depallens, O., 2012. Regulatory assessment of in vitro skin corrosion and irritation data within the European framework: Workshop recommendations. Regul Toxicol Pharmacol 62 (2), 393–403. https://doi.org/10.1016/j.yrtph.2011.10.015.
[23] Fadeel, B., Bussy, C., Merino, S., Vázquez, E., Flahaut, E., Mouchet, F., Evariste, L., Gauthier, L., Koivisto, A.J., Vogel, U., Martín, C., Delogu, L.G., Buerki-Thurnherr, T., Wick, P., Beloin-Saint-Pierre, D., Hischier, R., Pelin, M., Candotto Carniel, F., Tretiach, M., Bianco, A., 2018. Safety assessment of graphene-based materials: focus on human health and the environment. ACS Nano 12 (11), 10582–10620. https://doi.org/10.1021/acsnano.8b04758.
[24] FDA. (2019, September 2). *Guidance for Industry: Pyrogen and Endotoxins Testing: Questions and Answers*. FDA. ⟨https://www.fda.gov/regulatory-information/search-fda-guidance-documents/guidance-industry-pyrogen-and-endotoxins-testing-questions-and-answers⟩.
[25] Ferreira, C.J., Leitune, V.C.B., Balbinot, G. de S., Degrazia, F.W., Arakelyan, M., Sauro, S., Mezzomo Collares, F., 2019. Antibacterial and remineralizing fillers in experimental orthodontic adhesives. Mater (Basel, Switz) 12 (4), 652. https://doi.org/10.3390/ma12040652.
[26] Fiume, M.M., Bergfeld, W.F., Belsito, D.V., Hill, R.A., Klaassen, C.D., Liebler, D.C., Marks, J.G., Shank, R.C., Slaga, T.J., Snyder, P.W., Andersen, F.A., 2015. Safety assessment of boron nitride as used in cosmetics. Int J Toxicol 34 (3), 53S–60S. https://doi.org/10.1177/1091581815617793.
[27] Frankart, A., Coquette, A., Schroeder, K.-R., Poumay, Y., 2012. Studies of cell signaling in a reconstructed human epidermis exposed to sensitizers: IL-8 synthesis and release depend on EGFR activation. Arch Dermatol Res 304 (4), 289–303. https://doi.org/10.1007/s00403-012-1209-5.
[28] Fusco, L., Garrido, M., Martín, C., Sosa, S., Ponti, C., Centeno, A., Alonso, B., Zurutuza, A., Vázquez, E., Tubaro, A., Prato, M., Pelin, M., 2020. Skin irritation potential of graphene-based materials using a non-animal test. Nanoscale 12 (2), 610–622. https://doi.org/10.1039/c9nr06815e.
[29] Gangemi, S., Franchina, T., Minciullo, P.L., Profita, M., Zanghì, M., David, A., Kennez, I., Adamo, V., 2013. IL-33/IL-31 axis: A new pathological mechanisms for EGFR tyrosine kinase inhibitors-associated skin toxicity. J Cell Biochem 114 (12), 2673–2676. https://doi.org/10.1002/jcb.24614.
[30] Gibbs, S., 2009. In vitro irritation models and immune reactions. Ski Pharmacol Physiol 22 (2), 103–113. https://doi.org/10.1159/000178869.
[31] Golberg, D., Bando, Y., Huang, Y., Terao, T., Mitome, M., Tang, C., Zhi, C., 2010. Boron nitride nanotubes and nanosheets. ACS Nano 4 (6), 2979–2993. https://doi.org/10.1021/nn1006495.
[32] González, V.J., Rodríguez, A.M., Payo, I., Vázquez, E., 2020. Mechanochemical preparation of piezoelectric nanomaterials: BN, MoS2 and WS2 2D materials and their glycine-cocrystals. Nanoscale Horiz 5 (2), 331–335. https://doi.org/10.1039/C9NH00494G.
[33] He, H., Peng, W., Liu, J., Chan, X.Y., Liu, S., Lu, L., Le Ferrand, H., 2022. Microstructured BN composites with internally designed high thermal conductivity paths for 3D electronic packaging. Adv Mater (Deerfield Beach, Fla) 34 (38), e2205120. https://doi.org/10.1002/adma.202205120.
[34] Jensen, C., Teng, Y., 2020. Is it time to start transitioning from 2D to 3D cell culture? Front Mol Biosci 7. https://doi.org/10.3389/fmolb.2020.00033.
[35] Jiang, H., Cai, Q., Mateti, S., Yu, Y., Zhi, C., Chen, Y., 2021. Boron nitride nanosheet dispersion at high concentrations. ACS Appl Mater Interfaces 13 (37), 44751–44759. https://doi.org/10.1021/acsami.1c11795.
[36] Kalinski, P., 2012. Regulation of immune responses by prostaglandin E2. J Immunol 188 (1), 21–28. https://doi.org/10.4049/jimmunol.1101029.
[37] Kidd, D.A., Johnson, M., Clements, J., 2007. Development of an in vitro corrosion/irritation prediction assay using the EpiDerm skin model. Toxicol Vitr: Int J Publ Assoc BIBRA 21 (7), 1292–1297. https://doi.org/10.1016/j.tiv.2007.08.018.
[38] Kıvanç, M., Barutca, B., Koparal, A.T., Göncü, Y., Bostancı, S.H., Ay, N., 2018. Effects of hexagonal boron nitride nanoparticles on antimicrobial and antibiofilm activities, cell viability. Mater Sci Eng C, Mater Biol Appl 91, 115–124. https://doi.org/10.1016/j.msec.2018.05.028.
[39] Kostoglou, N., Polychronopoulou, K., Rebholz, C., 2015. Thermal and chemical stability of hexagonal boron nitride (h-BN) nanoplatelets. Vacuum 112, 42–45. https://doi.org/10.1016/j.vacuum.2014.11.009.
[40] Kostoglou, N., Stock, S., Solomi, A., Holzapfel, D.M., Hinder, S., Baker, M., Constantinides, G., Ryzhkov, V., Maletaskic, J., Matovic, B., Schneider, J.M., Rebholz, C., Mitterer, C., 2024. The roles of impurities and surface area on thermal stability and oxidation resistance of BN nanoplatelets. Article 7 Nanomaterials 14 (7). https://doi.org/10.3390/nano14070601.
[41] Lee, H.-Y., Shin, S.H.R., Abezgauz, L.L., Lewis, S.A., Chirsan, A.M., Danino, D.D., Bishop, K.J.M., 2013. Integration of gold nanoparticles into bilayer structures via adaptive surface chemistry. J Am Chem Soc 135 (16), 5950–5953. https://doi.org/10.1021/ja400225n.
[42] Lin, H., Buerki-Thurnherr, T., Kaur, J., Wick, P., Pelin, M., Tubaro, A., Carniel, F.C., Tretiach, M., Flahaut, E., Iglesias, D., Vázquez, E., Cellot, G., Ballerini, L., Castagnola, V., Benfenati, F., Armirotti, A., Sallustrau, A., Taran, F., Keck, M., Bianco, A., 2024. Environmental and health impacts of graphene and other two-dimensional materials: a graphene flagship perspective. ACS Nano 18 (8), 6038–6094. https://doi.org/10.1021/acsnano.3c09699.
[43] Liu, B., Zhou, K., 2019. Recent progress on graphene-analogous 2D nanomaterials: Properties, modeling and applications. Prog Mater Sci 100, 99–169. https://doi.org/10.1016/j.pmatsci.2018.09.004.
[44] Liu, S., Shen, Z., Wu, B., Yu, Y., Hou, H., Zhang, X.-X., Ren, H., 2017. Cytotoxicity and efflux pump inhibition induced by molybdenum disulfide and boron nitride nanomaterials with sheetlike structure. Environ Sci Technol 51 (18), 10834–10842. https://doi.org/10.1021/acs.est.7b02463.
[45] Lu, Z., Zhu, M., Liu, Y., Zhang, G., Tan, Z., Li, X., Xu, S., Wang, L., Dou, R., Wang, B., Yao, Y., Zhang, Z., Dong, J., Cheng, Z., Chen, S., 2022. Low-temperature synthesis of boron nitride as a large-scale passivation and protection layer for two-dimensional materials and high-performance devices. ACS Appl Mater Interfaces 14 (22), 25984–25992. https://doi.org/10.1021/acsami.2c02803.
[46] Lucherelli, M.A., Qian, X., Weston, P., Eredia, M., Zhu, W., Samorì, P., Gao, H., Bianco, A., von dem Bussche, A., 2021. Boron nitride nanosheets can induce water channels across lipid bilayers leading to lysosomal permeabilization. Adv Mater (Deerfield Beach, Fla) 33 (45), e2103137. https://doi.org/10.1002/adma.202103137.
[47] Martinez, V., Corsini, E., Mitjans, M., Pinazo, A., Vinardell, M.P., 2006. Evaluation of eye and skin irritation of arginine-derivative surfactants using different in vitro endpoints as alternatives to the in vivo assays. Toxicol Lett 164 (3), 259–267. https://doi.org/10.1016/j.toxlet.2006.01.005.
[48] Mohammadi, E., Nikbakht, F., Barati, M., Roghani, M., Vazifekhah, S., Khanizadeh, A.M., Heidari, Z., 2022. Protective effect of N-acetyl cysteine on the mitochondrial dynamic imbalance in temporal lobe epilepsy: Possible role of mTOR. Neuropeptides 96, 102294. https://doi.org/10.1016/j.npep.2022.102294.
[49] Molaei, M.J., Younas, M., Rezakazemi, M., 2021. A comprehensive review on recent advances in two-dimensional (2D) hexagonal boron nitride. ACS Appl Electron Mater 3 (12), 5165–5187. https://doi.org/10.1021/acsaelm.1c00720.
[50] Mukheem, A., Shahabuddin, S., Akbar, N., Miskon, A., Muhamad Sarih, N., Sudesh, K., Ahmed Khan, N., Saidur, R., Sridewi, N., 2019. Boron nitride doped polyhydroxyalkanoate/chitosan nanocomposite for antibacterial and biological applications. Article 4. Nanomaterials 9 (4). https://doi.org/10.3390/nano9040645.
[51] Mukherjee, S.P., Lozano, N., Kucki, M., Rio-Castillo, A.E.D., Newman, L., Vázquez, E., Kostarelos, K., Wick, P., Fadeel, B., 2016. Detection of endotoxin contamination of graphene based materials using the TNF-α expression test and guidelines for endotoxin-free graphene oxide production. PLOS ONE 11 (11), e0166816. https://doi.org/10.1371/journal.pone.0166816.
[52] Nedunchezhian, K., Aswath, N., Thiruppathy, M., Thirugnanamurthy, S., 2016. Boron neutron capture therapy—a literature review. J Clin Diagn Res: JCDR 10 (12), ZE01–ZE04. https://doi.org/10.7860/JCDR/2016/19890.9024.
[53] Netzlaff, F., Lehr, C.-M., Wertz, P.W., Schaefer, U.F., 2005. The human epidermis models EpiSkin®, SkinEthic® and EpiDerm®: An evaluation of morphology and their suitability for testing phototoxicity, irritancy, corrosivity, and substance transport. Eur J Pharm Biopharm 60 (2), 167–178. https://doi.org/10.1016/j.ejpb.2005.03.004.
[54] Norman, K.G., Canter, J.A., Shi, M., Milne, G.L., Morrow, J.D., Sligh, J.E., 2010. Cyclosporine A suppresses keratinocyte cell death through MPTP inhibition in a model for skin cancer in organ transplant recipients. Mitochondrion 10 (2), 94–101. https://doi.org/10.1016/j.mito.2009.10.001.
[55] OECD, 2019. *Test No. 431: In vitro skin corrosion: reconstructed human epidermis (RHE) test method*. Organisation for Economic Co-operation and Development. https://doi.org/10.1787/9789264264618-en.
[56] OECD. (2021). *Test No. 439: In Vitro Skin Irritation: Reconstructed Human Epidermis Test Method*. Organisation for Economic Co-operation and Development. ⟨https://www.oecd-ilibrary.org/environment/test-no-439-in-vitro-skin-irritation-reconstructed-human-epidermis-test-method_9789264242845-en⟩.
[57] Parish, S.T., Aschner, M., Casey, W., Corvaro, M., Embry, M.R., Fitzpatrick, S., Kidd, D., Kleinstreuer, N.C., Lima, B.S., Settivari, R.S., Wolf, D.C., Yamazaki, D., Boobis, A., 2020. An evaluation framework for new approach methodologies (NAMs) for human health safety assessment. Regul Toxicol Pharmacol 112, 104592. https://doi.org/10.1016/j.yrtph.2020.104592.
[58] Pasparakis, M., Haase, I., Nestle, F.O., 2014. Mechanisms regulating skin immunity and inflammation. Nat Rev Immunol 14 (5), 289–301. https://doi.org/10.1038/nri3646.
[59] Pelin, M., Fusco, L., León, V., Martín, C., Criado, A., Sosa, S., Vázquez, E., Tubaro, A., Prato, M., 2017. Differential cytotoxic effects of graphene and graphene oxide on skin keratinocytes. Sci Rep 7, 40572. https://doi.org/10.1038/srep40572.
[60] Pelin, M., Fusco, L., Martín, C., Sosa, S., Frontiñán-Rubio, J., González-Domínguez, J.M., Durán-Prado, M., Vázquez, E., Prato, M., Tubaro, A., 2018.

Graphene and graphene oxide induce ROS production in human HaCaT skin keratinocytes: The role of xanthine oxidase and NADH dehydrogenase. Nanoscale 10 (25), 11820–11830. https://doi.org/10.1039/c8nr02933d.

[61] Pelin, M., Passerino, C., Rodríguez-Garraus, A., Carlin, M., Sosa, S., Suhonen, S., Vales, G., Alonso, B., Zurutuza, A., Catalán, J., Tubaro, A., 2023. Role of chemical reduction and formulation of graphene oxide on its cytotoxicity towards human epithelial bronchial cells. Article 15 Nanomaterials 13 (15). https://doi.org/10.3390/nano13152189.

[62] Pelin, M., Sosa, S., Prato, M., Tubaro, A., 2018. Occupational exposure to graphene based nanomaterials: Risk assessment. Nanoscale 10 (34), 15894–15903. https://doi.org/10.1039/C8NR04950E.

[63] Pellevoisin, C., Videau, C., Briotet, D., Grégoire, C., Tornier, C., Alonso, A., Rigaudeau, A.S., Bouez, C., Seyler, N., 2018. SkinEthic™ RHE for in vitro evaluation of skin irritation of medical device extracts. Toxicol Vitr 50, 418–425. https://doi.org/10.1016/j.tiv.2018.01.008.

[64] Qiu, K., Zou, W., Fang, Z., Wang, Y., Bell, S., Zhang, X., Tian, Z., Xu, X., Ji, B., Li, D., Huang, T., Diao, J., 2023. 2D MoS2 and BN nanosheets damage mitochondria through membrane penetration. ACS Nano 17 (5), 4716–4728. https://doi.org/10.1021/acsnano.2c11003.

[65] Ricotti, L., Fujie, T., Vazão, H., Ciofani, G., Marotta, R., Brescia, R., Filippeschi, C., Corradini, I., Matteoli, M., Mattoli, V., Ferreira, L., Menciassi, A., 2013. Boron nitride nanotube-mediated stimulation of cell co-culture on micro-engineered hydrogels. PLOS ONE 8 (8), e71707. https://doi.org/10.1371/journal.pone.0071707.

[66] Roy, S., Deo, K.A., Singh, K.A., Lee, H.P., Jaiswal, A., Gaharwar, A.K., 2022. Nano-bio interactions of 2D molybdenum disulfide. Adv Drug Deliv Rev 187, 114361. https://doi.org/10.1016/j.addr.2022.114361.

[67] Roy, S., Zhang, X., Puthirath, A.B., Meiyazhagan, A., Bhattacharyya, S., Rahman, M.M., Babu, G., Susarla, S., Saju, S.K., Tran, M.K., Sassi, L.M., Saadi, M. a S.R., Lai, J., Sahin, O., Sajadi, S.M., Dharmarajan, B., Salpekar, D., Chakingal, N., Baburaj, A., Ajayan, P.M., 2021. Structure, properties and applications of two-dimensional hexagonal boron nitride. Adv Mater (Deerfield Beach, Fla) 33 (44), e2101589. https://doi.org/10.1002/adma.202101589.

[68] Sebastiani, S., Albanesi, C., De Pità, O., Puddu, P., Cavani, A., Girolomoni, G., 2002. The role of chemokines in allergic contact dermatitis. Arch Dermatol Res 293 (11), 552–559. https://doi.org/10.1007/s00403-001-0276-9.

[69] Şen, Ö., Culha, M., 2016. Boron nitride nanotubes included thermally cross-linked gelatin–glucose scaffolds show improved properties. Colloids Surf B: Biointerfaces 138, 41–49. https://doi.org/10.1016/j.colsurfb.2015.11.036.

[70] Şen, Ö., Emanet, M., Çulha, M., 2019. Stimulatory effect of hexagonal boron nitrides in wound healing. ACS Appl Bio Mater 2 (12), 5582–5596. https://doi.org/10.1021/acsabm.9b00669.

[71] Sharker, S.M., 2019. Hexagonal boron nitrides (white graphene): a promising method for cancer drug delivery. Int J Nanomed 14, 9983–9993. https://doi.org/10.2147/IJN.S205095.

[72] Soiferman, D., Ayalon, O., Weissman, S., Saada, A., 2014. The effect of small molecules on nuclear-encoded translation diseases. Biochimie 100, 184–191. https://doi.org/10.1016/j.biochi.2013.08.024.

[73] Song, L., Ci, L., Lu, H., Sorokin, P.B., Jin, C., Ni, J., Kvashnin, A.G., Kvashnin, D.G., Lou, J., Yakobson, B.I., Ajayan, P.M., 2010. Large Scale Growth and Characterization of Atomic Hexagonal Boron Nitride Layers. Nano Lett 10 (8), 3209–3215. https://doi.org/10.1021/nl1022139.

[74] Spiekstra, S.W., Toebak, M.J., Sampat-Sardjoepersad, S., van Beek, P.J., Boorsma, D.M., Stoof, T.J., von Blomberg, B.M.E., Scheper, R.J., Bruynzeel, D.P., Rustemeyer, T., Gibbs, S., 2005. Induction of cytokine (interleukin-1alpha and tumor necrosis factor-alpha) and chemokine (CCL20, CCL27, and CXCL8) alarm signals after allergen and irritant exposure. Exp Dermatol 14 (2), 109–116. https://doi.org/10.1111/j.0906-6705.2005.00226.x.

[75] Taskin, I.C., Sen, O., Emanet, M., Culha, M., Yilmaz, B., 2020. Hexagonal boron nitrides reduce the oxidative stress on cells. Nanotechnology 31 (21), 215101. https://doi.org/10.1088/1361-6528/ab6fdc.

[76] Teo, W.Z., Chng, E.L.K., Sofer, Z., Pumera, M., 2014. Cytotoxicity of exfoliated transition-metal dichalcogenides (MoS2, WS2, and WSe2) is lower than that of graphene and its analogues. Chem – A Eur J 20 (31), 9627–9632. https://doi.org/10.1002/chem.201402680.

[77] Umrao, S., Maurya, A.K., Shukla, V., Grigoriev, A., Ahuja, R., Vinayak, M., Srivastava, R.R., Saxena, P.S., Oh, I.-K., Srivastava, A., 2019. Anticarcinogenic activity of blue fluorescent hexagonal boron nitride quantum dots: as an effective enhancer for DNA cleavage activity of anticancer drug doxorubicin. Mater Today Bio 1, 100001. https://doi.org/10.1016/j.mtbio.2019.01.001.

[78] Vereinte Nationen (Ed.). (2021). *Globally harmonized system of classification and labelling of chemicals (GHS)*. United Nations.

[79] Wu, K., Yu, L., Lei, C., Huang, J., Liu, D., Liu, Y., Xie, Y., Chen, F., Fu, Q., 2019. Green production of regenerated cellulose/boron nitride nanosheet textiles for static and dynamic personal cooling. ACS Appl Mater Interfaces 11 (43), 40685–40693. https://doi.org/10.1021/acsami.9b15612.